Environmental Research 136 (2015) 253–263

Contents lists available at ScienceDirect

Environmental Research

journal homepage: www.elsevier.com/locate/envres

Silver nanoparticles affect on gene expression of inflammatory and neurodegenerative responses in mouse brain neural cells

Chin-Lin Huang, I-Lun Hsiao, Ho-Chen Lin, Chu-Fang Wang, Yuh-Jeen Huang*, Chun-Yu Chuang*

Department of Biomedical Engineering and Environmental Sciences, National Tsing Hua University, 101, Section 2, Kuang-Fu Road, Hsinchu 30013, Taiwan

ARTICLE INFO

Article history:
Received 15 July 2014
Received in revised form
3 November 2014
Accepted 5 November 2014
Available online 20 November 2014

Keywords:
Silver nanoparticle
Inflammation
Gene expression
Neurodegenerative disorder
Alzheimer 's disease

ABSTRACT

Silver nanoparticles (AgNPs) have antibacterial characteristics, and currently are applied in Ag-containing products. This study found neural cells can uptake 3–5 nm AgNPs, and investigated the potential effects of AgNPs on gene expression of inflammation and neurodegenerative disorder in murine brain ALT astrocytes, microglial BV-2 cells and neuron N2a cells. After AgNPs (5, 10, 12.5 μg/ml) exposure, these neural cells had obviously increased IL-1β secretion, and induced gene expression of C-X-C motif chemokine 13 (*CXCL13*), macrophage receptor with collagenous structure (*MARCO*) and glutathione synthetase (*GSS*) for inflammatory response and oxidative stress neutralization. Additionally, this study found amyloid-β (Aβ) plaques for pathological feature of Alzheimer's disease (AD) deposited in neural cells after AgNPs treatment. After AgNPs exposure, the gene expression of amyloid precursor protein (*APP*) was induced, and otherwise, neprilysin (*NEP*) and low-density lipoprotein receptor (*LDLR*) were reduced in neural cells as well as protein level. These results suggested AgNPs could alter gene and protein expressions of Aβ deposition potentially to induce AD progress in neural cells. It's necessary to take notice of AgNPs distribution in the environment.

1. Introduction

In recent years, nanotechnology grows rapidly, and nanoparticles are produced and widely utilized in diverse areas of different industrial applications because of its high interfacial reactivity and unique physicochemical properties (Loo et al., 2013). As to antibacterial/antifungal characteristics, silver nanoparticles (AgNPs) have been used in clothes, cosmetics, wound dressing, air-freshener sprays, water disinfectant, sunscreens, hygiene products and food containers, which increases the release of nanoparticles to environment and may cause exposure to human (Ribeiro et al., 2013). The exposure route for AgNPs happens via ingestion, inhalation or dermal contact. Kulthong et al. (2010) indicated that the antibacterial fabric from six commercial fabrics releases silver of AgNPs when is immersed in artificial sweat as a model to represent the human skin environment. In addition, AgNPs may have an access to systemic circulation through broken skin when we use the AgNP-containing products such as bandages or wound dressings (Singh and Ramarao, 2012). After injection different particles size of Ag (nanosized and microsized) in rats (62.8 mg/kg), AgNPs can translocate to the blood circulation and distribute throughout the main organs, especially in the kidney, liver, spleen, lung and brain, and induce blood–brain barrier (BBB) destruction and astrocyte swelling to cause neuronal degeneration (Tang et al., 2009).

Ag is one of the most toxic metals for the marine systems (Tappin et al., 2010), and the monovalent silver ion is considered as the most toxic silver species in aquatic systems and causes intracellular accumulation in phytoplankton (Lee et al., 2005). However, the AgNPs (< 100 nm, 0.5 and 1 μg/ml) cause nuclear condensation and induce higher dramatically cytotoxicity than Ag ions in human lymphoma cells (Eom and Choi, 2010). In addition, a proteomic analysis showed that 20 nm AgNPs interfere with protein regulations of mitochondrial translation, RNA processing, tRNA metabolism and cell proliferation more than Ag ions and larger size AgNPs (100 nm) in human colon adenocarcinoma LoVo cells (Verano-Braga et al., 2014). The diameter 139 ± 37 nm AgNPs trigger dose-dependent effect of decreased cell viability on human lung carcinoma A549 cells in exposure to 5, 10 and 15 μg/ml AgNPs (Foldbjerg et al., 2011). Besides, the cell deaths in apoptosis and necrosis all increase after exposure to AgNPs (2.5, 5, 10 and 15 μg/ml). Moreover, Gaiser et al. (2013) pointed that 20 nm

* Corresponding authors. Fax: +886 3 5718649.
E-mail addresses: yjhuang@mx.nthu.edu.tw (Y.-J. Huang), cychuang@mx.nthu.edu.tw (C.-Y. Chuang).

http://dx.doi.org/10.1016/j.envres.2014.11.006

diameter nanoparticles can cause toxicity, inflammation and oxidative stress after exposure to human C3A hepatocytes and female Wistar rats. Besides, the inflammatory cytokines, e.g., IL-8, MIP2, IL-1RI and TNF-α, are both increased on in vitro and in vivo models after AgNPs-induction. Overall, the Ag and Cu nanoparticles can easily enter the mice brain to disrupt BBB permeability and induce neurotoxicity, which alters brain sensory, motor and cognitive functions (Sharma and Sharma, 2012). AgNPs (20 nm; 1, 5, 10 and 50 μg/ml) can reduce cell viability in primary rat cortical cells, and inhibit the sprouting of neuronal branches and elongation of neuritis for fragmentation and degeneration of mature neurons (Xu et al., 2013).

Brain is composed of endothelial cells, neurons and glial cells. Astrocytes are known as reactive astrogliosis cells to regulate metal homeostasis, supply nutrients to neurons and protect other brain cells against oxidative stress and metal toxicity (Sofroniew and Vinters, 2010). Microglias are a type of glial cell major brain-resident macrophage-like cells in the central nerve system (CNS) to defense against microorganism invasion and injury, and release some cytokine factors to mediate neuroinflammatory processes (Wang et al., 2011). The inflammatory response, a tissue reaction to injury or an antigen, releases cytokines, chemokines, reactive oxygen species (ROS) and nitric oxides (NO) (Wei et al., 2013). Nerve cells connect to each other to form neural networks. Neurons are electrically excitable brain endothelium to transmit information through electrical and chemical signals via synapses and contact with perivascular astrocytes and pericytes (Weiss et al., 2009). Tang et al. (2010) indicated that AgNPs can cross through the BBB of rat brain to influence brain cells through transcytosis of capillary endothelial cells detectable by transmission electronic microscopy (TEM) and inductively-coupled plasma mass spectrometry (ICP-MS). Thus, the highest concentration of silver is observed in the kidneys and brain 28 days after injection a dose 5 mg kg^{-1} bw AgNPs (20 and 200 nm) in Wistar rats. Dziendzikowska et al. (2012) found that AgNPs increase ROS generation and heme oxygenase 1 (HO-1) protein expression to cause neuronal oxidative damage and directly interfere with calcium responses in primary mixed neural cells. Increased levels of ROS occurred chronically in the early disease, which is relevant to neurodegenerative disorders, such as Alzheimer's and Parkinson's disease (Smith and Cass, 2007). Moreover, glutathione metabolism plays an important role of protecting cell from oxidative stress, and their gene expression related to oxidative stress are significantly altered in the caudate, frontal cortex and hippocampus of male C57BL/6N mice after administered 25 nm AgNPs (Rahman et al., 2009).

The C-X-C motif chemokine 13 (*CXCL13*) play a role in the B-cell recruitment and distribution, associated with chronic inflammatory process (Nakajima et al., 2008). Macrophage receptor with collagenous structure (*MARCO*) is important for immune responses to bacterial infections by mediating the binding and phagocytosis of pathogens (Komine et al., 2013). Accordingly, studies have indicated that AgNPs can induce ROS and cytokines increasing and then cause inflammatory response. As *CXCL13* and *MARCO* genes are immune mediators in response to inflammation, exposure to AgNPs may change their gene expression. Moreover, glutathione synthetase (GSS) can synthesize glutathione (GSH) potentially to inhibit oxidative stress and prevent cellular damage from free radicals and peroxides (Koike et al., 2013), and AgNPs exposure probably alters *GSS* gene expression.

Amyloid beta (Aβ) is a peptide of amino acids that is processed from amyloid precursor protein (APP). Aβ protein is considered the main responsible for neurodegenerative disorder such as Alzheimer's disease (AD). The up-regulation of *APP* gene expression interferes with Aβ metabolism underlying the pathogenesis of AD (Dong et al., 2012). Low-density lipoprotein receptor (LDLR) enhances Aβ uptake and degradation through binding Aβ and Aβ/ApoE complex (Basak et al., 2012). Thus, the down-regulation of *LDLR* gene leads Aβ deposition. Besides, neprilysin (NEP) is a major Aβ-degrading enzyme in brain to degrade Aβ protein (El–Amouri et al., 2007). Sequentially, it is important to investigate the receptors and gene expression regulating Aβ amyloid internalization in neural cells for understanding the AD pathogenesis.

According to previous studies, the information until now is not well known that whether the AgNPs-induced neuroinflammation cause the changes in gene expression related neurodegenerative disorder such as AD. In this study, we investigated whether the 3–5 nm AgNPs can pass through mouse brain neuronal cells and induce Aβ amyloid generation underlying the potential effect of AgNPs on gene expression of inflammatory response, oxidative stress, and Aβ deposition.

2. Material and methods

2.1. Cell culture and exposure

This study used three types of neural cells, murine brain ALT astrocytes (BCRC 60581), murine microglial BV-2 cells (ICLC ATL03001) and mouse neuroblastoma Neuro-2a (N2a) cells (BCRC 60026). N2a cells were cultured in high glucose Dulbecco's Modified Eagle's Medium (DMEM; CORNING, New York) supplemented with 10 percent fetal bovine serum (Invitrogen, Carlsbad, Canada), 1 percent antibiotic (Biowest, Loire Valley, France), 1 percent L-glutamine (Invitrogen), 1 percent sodium pyruvate (Invitrogen) in a cell incubator with 5 percent CO_2 at 37 °C. ALT cells and BV-2 cells were cultured in the similar medium with N2a cells except for the lack of 1 percent sodium pyruvate. When N2a cells grew to 70–80 percent confluence of a culture plate, the growth medium was removed and replaced with differentiation medium for two days. The differentiation medium containing forskolin and isobutylmethylxanthine (IBMX) was added to N2a cells for 24 h differentiation. N2a cells can be differentiated into a neuron-like morphology with expression of several neuronal markers. The 3–5 nm AgNPs were produced by a physical method without surfactants or stabilizers (Gold Nanotech Inc., Taiwan). AgNPs (0.5, 1, 5, 10 and 12.5 μg/ml) and lipopolysaccharides (LPS; 0.2 and 2 μg/ml; Invitrogen) were respectively added into the medium to treat ALT, BV-2 and N2a cells for 24 h exposure.

2.2. Polarizing microscope

N2a cells were cultured on glass coverslips with the treatment of AgNPs (5 nm, 12.5 μg/ml) for 24 h. After treatment, the cells on coverslips were fixed in 4 percent paraformaldehyde (PFA) for 10 min at 4 °C, then washed with phosphate buffered saline (PBS) and mounted with slides in mountain medium. Images of AgNPs location were captured under the polarizing microscopy (IX71, Olympus, Tokyo, Japan).

2.3. Cell proliferation of neural cells

The neural cells 1×10^4 cm^{-2} were seeded in 96-well plates for cell viability analysis. After exposure to AgNPs or LPS, the suspensions were discarded, alamarBlue® reagent (DMEM/10 percent FBS 1:10; Invitrogen) was added as a cell viability indicator followed by a 2 h incubation at 37 °C, and the absorbance was monitored at 570 nm using 600 nm as a reference wavelength. The cell viability was calculated as [cell number of exposure samples]/[cell number of control] × 100. Cell numbers were derived from a standard curve, which was obtained after seeding serially diluted cells (from 5×10^4 to 1.56×10^3 cells/ml) in a 96-well plate.

2.4. Cytokine assay of IL-1β

The concentrations of pro-inflammatory cytokine IL-1β were determined using ELISA kits (Mouse IL-1β Instant ELISA, eBioscience, San Diego, Canada) according to the operation manual. A 96-well plate was coated with capture antibody (purified anti-mouse IL-1β) in coating buffer and incubated overnight at 4 °C. After three time wash with PBST (PBS with 1 percent Tween 20), the blocking solution (200 μl) was added to each well with 1 h. After wash, the samples (100 μl) and IL-1β standards (16–2000 pg/ml) were added to each well for 2 h incubation at room temperature. After incubation and wash, the 100 ul of biotin-conjugated anti-mouse IL-1β and streptavidin–horseradish peroxidase (HRP) were added to each well for 30 min incubation, then wash, and each well was added to 100 μl TMB (3,3′,5,5′-Tetramethylbenzidine) substrate solution for 15 min. Final, the 50 μl stop solution (2 M H_2SO_4) was added to each well and the optical density was determined at 450 nm using a VERSAmax microplate reader (Molecular Devices, Sunnyvale, Canada).

2.5. Immunofluorescent detection of Aβ protein

N2a cells cultured on coverslips were washed twice with 1X PBS and then fixed with 4 percent PFA for 10 min at 4 °C, and washed with PBS. Cells were permeabilized with 0.1 percent Triton X-100/PBS solution at room temperature for 30 min, blocked in 2 percent horse serum (HS) at room temperature for 30 min, and then incubated for 1 h respectively with primary rabbit anti-mouse $A\beta_{1-40}$ (1:500; Cat. 171608, Merck Millipore, Darmstadt, Germany) or primary rabbit anti-mouse $A\beta_{1-42}$ (1:500; Cat. 171609, Merck Millipore). The coverslips were then washed three times with PBS and stained with secondary fluorescein isothiocyanate (FITC)-conjugated goat anti-rabbit IgG (1:500; Cat. 12-507, Merck Millipore). After washed in PBS, the coverslips were incubated with Hoechst 33258 (1:20; Cat. 23491-45-4, Sigma-Aldrich, St. Louis, MO) and rinsed in PBS. Coverslips were mounted on slides in mountain medium. Immunofluorescence images were captured with an inverted microscope with fluorescence filters (Axio Observer A1/D1, Zeiss, Oberkochen, Germany).

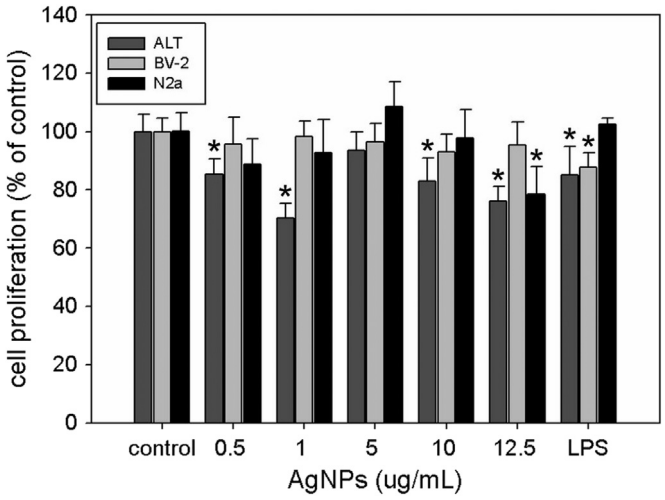

Fig. 2. Cell proliferation after exposure to AgNPs and LPS. Neural cells were treated with different concentration of 3–5 nm AgNPs (0.5, 1, 5, 10 and 12.5 μg/ml) and LPS (ALT 2 μg/ml, BV-2 0.2 μg/ml and N2a 2 μg/ml) for 24 h. The data were presented as mean ± SD ($n=3$). Asterisk indicates significant difference at $p<0.05$ compared with control. ALT: astrocyte, BV-2: microglia, and N2a: neuron cells.

2.6. RNA extraction

Total RNA was isolated respectively from ALT, BV-2 and N2a cells in exposure to AgNPs after 24 h using RNA Trizol (Invitrogen). After the culture medium were removed, neural cells were dissolved in 1 ml of TRIzol reagent, and then 0.2 ml chloroform was added a 1.5 ml eppendorf tube. The mixture was shook vigorously for 15 s and centrifuged at 12,000*g* for 15 min at 4 °C. Next, the supernatant was transferred to a fresh tube, and 0.5 ml isopropanol (SIGMA) was added at room temperature for 10 min. The

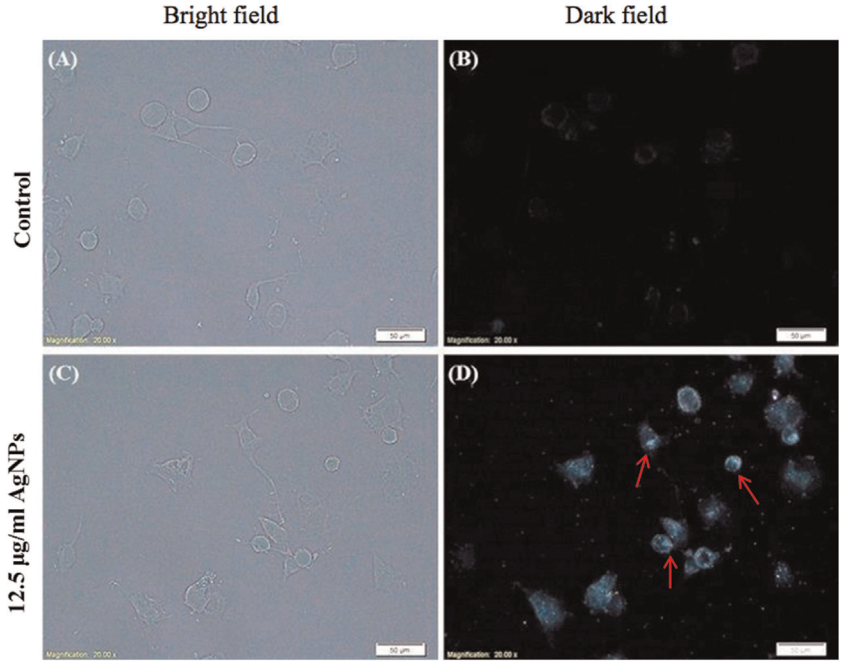

Fig. 1. AgNPs uptake in mouse neuron N2a cells. A polarizing microscope was used to detect 5 nm AgNPs distribution in N2a cells. N2a cells were (A, B) cultured in normal culture medium, or (C, D) exposed to 12.5 μg/ml AgNPs for 24 h. The bright field (A, C) and the dark field (B, D) indicate phase contrast image and polarizing image of corresponding cells respectively undertaken in 200× magnification with 30 μs and 10 ms exposure time. The red arrows point the location of AgNPs reflecting the bright spots mainly located inside the neural cells. (For interpretation of the references to color in this figure legend, the reader is referred to the web version of this article.)

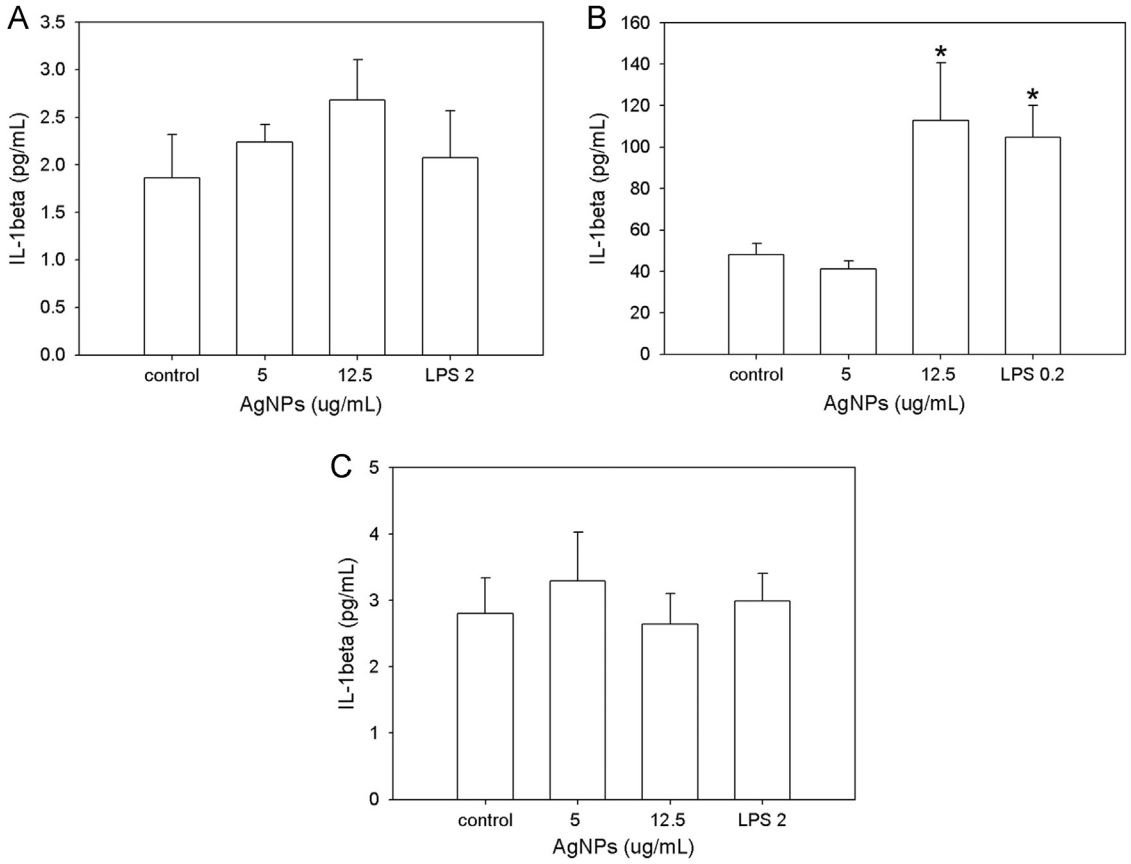

Fig. 3. Cytokines IL-1β in neural cells after exposure to AgNPs and LPS. (A) ALT, (B) BV-2 and (C) N2a cells were respectively treated with different concentrations of 3–5 nm AgNPs (5 and 12.5 μg/ml) and LPS (ALT 2 μg/ml, BV-2 0.2 μg/ml and N2a 2 μg/ml) for 24 h. The data were presented as mean ± SD ($n=3$). Asterisk indicates significant difference at $p<0.05$ compared with control. ALT: astrocyte, BV-2: microglia, and N2a: neuron cells.

RNA was precipitated after centrifugation at 12,000*g* for 10 min at 4 °C. The RNA pellet was washed with 1 ml of 75 percent ethanol (Taiwan Tobacco & Liquor Corporation, Taipei, Taiwan) and centrifuged at 7500*g* for 5 min at 4 °C to remove the ethanol. The RNA pellet was dried up and diluted with RNase-free water.The purified RNA was quantified using Nanodrop 2000c (Thermo, Wilmington, Massachusetts).

2.7. Reverse transcription polymerase chain reaction (RT-PCR)

cDNA was synthesized from total RNA by a high-capacity cDNA reverse transcription kit (Applied Biosystems, California). The 3 μg RNA was added 1.0 μl MultiScribe™ reverse transcriptase (50 unit μL^{-1}), 2.0 μl 10 × RT random primers, 0.8 μl 20 × concentrated dNTP mix, 2.0 μl 10 × concentrated RT buffer and RNase free water (DEPC water) in a 0.2 ml PCR tube, and subsequently amplified by PCR with one cycle of 20 °C 10 min, 37 °C 120 min and 85 °C 5 s.

2.8. Real time PCR for gene expression quantitation

One hundred nanograms cDNA was a was amplified by PCR with 40 cycles of denaturing (95 °C, 15 s), annealing (55 °C, 30 s) and extension (72 °C, 45 s) using 2 × power SYBR green PCR master mix (Applied Biosystems). PCR primers: *CXCL13* sense 5′-ATG TGT GAA TCC TCG TGC CAA-3′ and anti-sense 5′-AAA AAA GGT GCA GGT GTG TCT-3′; *MARCO* sense 5′-GGG TCA AAA AGG CGA ATC T-3′ and anti-sense 5′-ATG TTC CCA GAG CCA CCT-3′; *GSS* sense 5′-GGT ATC TTC CCT CAG CAG CCT T-3′ and anti-sense 5′-GCT TCC ATT CCC ACA CTC CAA A-3′; *APP* sense 5′-CTG GAC GGT TCG GGC TCT-3′ and anti-sense 5′-CGG GTC TGA CTC CCA CTT TC-3′; *LDLR* sense 5′-TCC AAT CAA TTC AGC TGT GGA G-3′ and anti-sense 5′-ATC AGA GCC ATC TAG GCA ATC TCG-3′; *NEP* sense 5′-AAA GCC AAA GAA GAA ACA GCG A-3′ and anti-sense 5′-GCA TAG AGA GCG ATC ATT GTC ACC G-3′; *β-actin* sense 5′-ATG CTC CCC GGG CTG TAT-3′ and anti-sense 5′-CCA CTG CTC CGG GTC TCG-3′. Quantitative analysis of PCR products was carried out by a sequence detector (Model 7300, Applied Biosystems) according to the manufacturer's instruction. The signal of SYBR green was measured at 530 nm during extension phase, and collected and analyzed with SDS 1.0 software. The threshold cycle (Ct) value denotes the cycle number at which the fluorescence generated within a reaction across the threshold, thus the Ct value is at the point accumulated a sufficient number of amplicons during the reaction. The relative level of mRNA expression is a ratio of optical density of the experimental groups to that of *β-actin* (internal control, an endogenous house-keeping gene). The relative Ct value of different condition was compared to that of control cells as reference to estimate the fold change of mRNA expression among the samples. Triplicates were performed for each primer pair.

2.9. Western blotting for protein determination

N2a cells were lysed with RIPA buffer (Cell Signaling, Danvers, MA) containing proteinase inhibitor Cocktail (Sigma), and centrifuged at 8000*g* for 3 min at 4 °C. Protein samples in the supernatant were immediately transferred, and the concentration was measured using a Bicinchoninic Acid Protein Assay Kit (Sigma). Protein in the samples were then electrophoresed over a 10% sodium dodecyl sulfate polyacrylamide gel, and subsequently transferred to a hydrophobic PVDF membrane (Millipore). The membrane-bound proteins were respectively immunostained

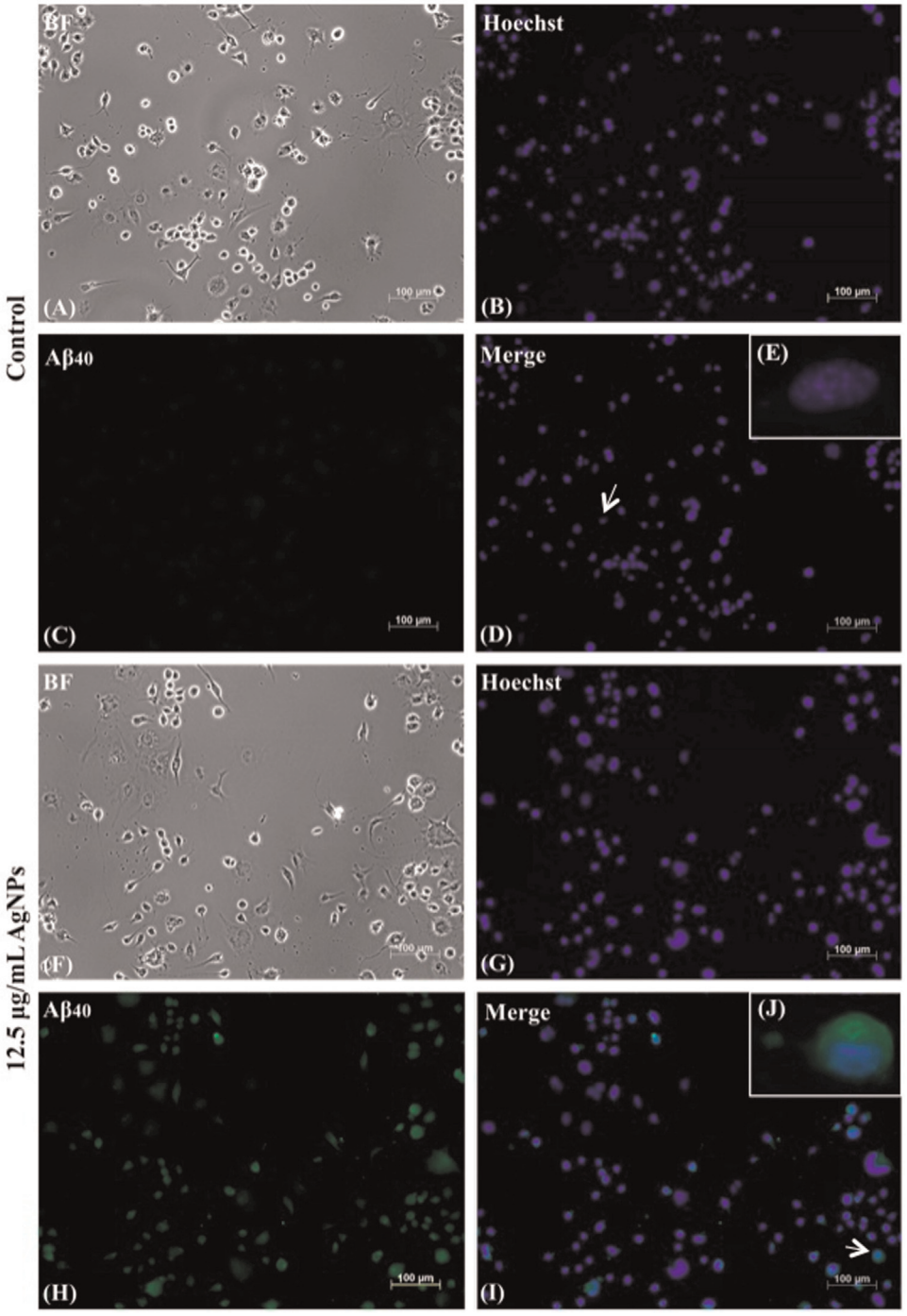

Fig. 4. Amyloid-β_{1-40} plaques inside mouse neuron N2a cells in exposure to AgNPs. Immunofluorescent detection of primary rabbit anti-mouse $A\beta_{1-40}$ was stained with secondary goat FITC-conjugated anti-rabbit IgG in N2a cells after 24 h 12.5 μg/ml 3–5 nm AgNPs treatment. The control groups (A–D) and AgNPs exposure groups (F–I) were taken under 100 × magnification respectively at 172 ms, 120 ms and 500 ms exposure time for bright field (BF), hoechst, and primary rabbit anti-mouse $A\beta_{1-40}$. (E) and (J) were a single cell image respectively according to (D) and (I) fields taken under 400 × magnification. The white arrows pointed out the view of 400 × images where are selected from 100 × ones.

with 1:1000 primary rabbit anti-mouse NEP (CD10) (Cat. EPR 2997, Abcam, Cambridge, MA), APP (Cat. EPR 5118-34, Abcam), LDLR (Cat. EP 155311, Abcam) or β-actin (Senta Cruz Biotechnlogy, Senta Cruz, CA) antibody and followed by treatment with secondary anti-rabbit IgG horseradish peroxidase (HRP) antibody (Senta Cruz Biotechnlogy, CA). The tagged proteins were detected using a chemiluminescence reagent (Thermo Scientific, Rockford, IL) and photographed in a G:Box ChemiXT 16 system (Syngene, Frederick, MD). The band intensities in the western blots were quantified by ImageJ software.

2.10. Statistical analysis

Results were described as mean ± standard deviation. Data analysis was conducted by the statistical package SPSS 13.0 (SPSS Inc., Chicago, Illinois). The statistically significant differences of cell proliferation, IL-1β, gene expression and protein respectively between AgNPs treatment and control were analyzed using Student's *t* test. All statistical significances were determined at two-tailed p value < 0.05.

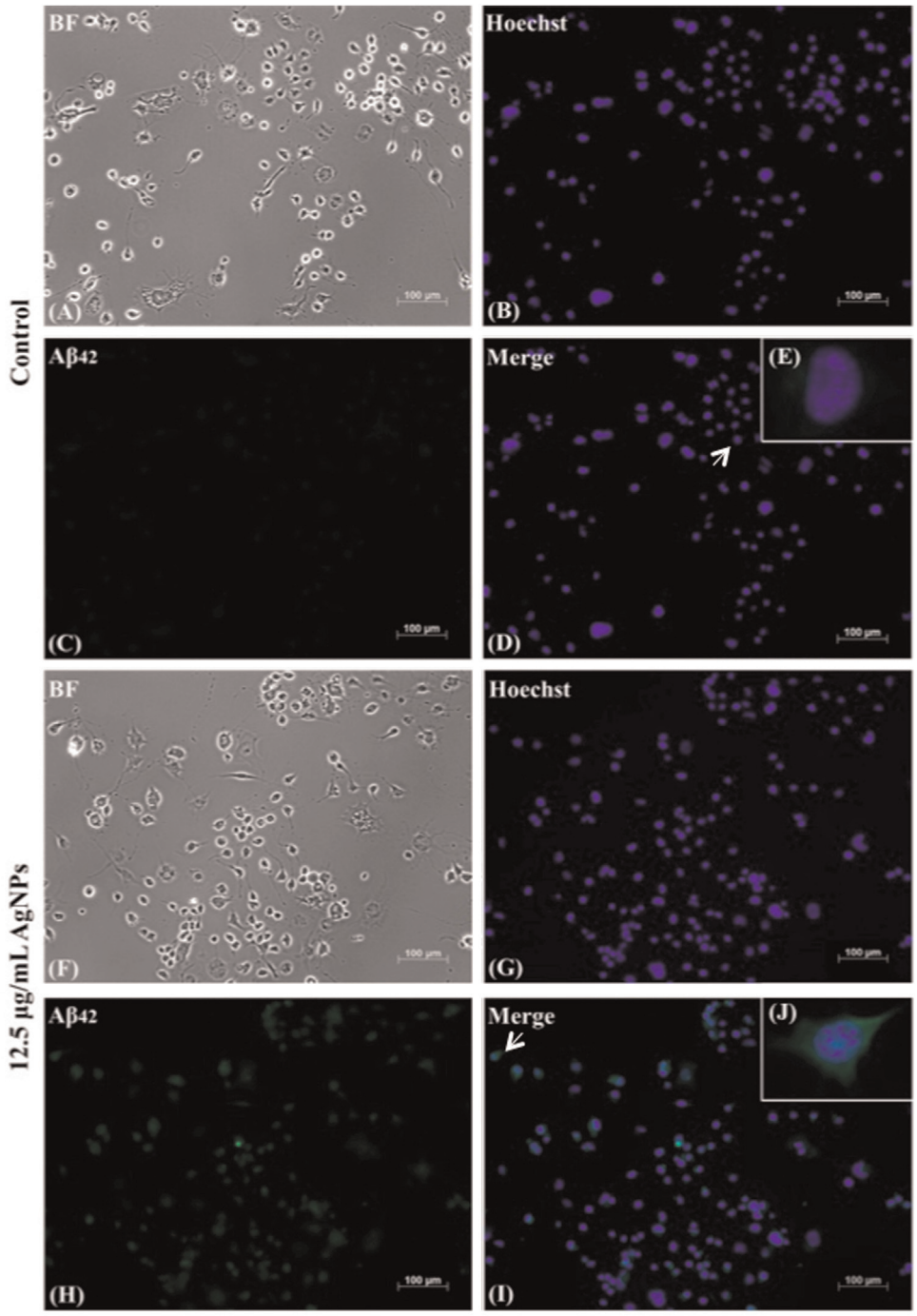

Fig. 5. Amyloid-β_{1-42} plaques inside mouse neuron N2a cells in exposure to AgNPs. Immunofluorescent detection of primary rabbit anti-mouse $A\beta_{1-42}$ was stained with secondary goat FITC-conjugated anti-rabbit IgG in N2a cells after 24 h 12.5 μg/ml 3–5 nm AgNPs treatment. The control groups (A–D) and AgNPs exposure groups (F–I) were taken under 100 × magnification respectively at 172 ms, 120 ms and 500 ms exposure time for bright field (BF), hoechst, and primary rabbit anti-mouse $A\beta_{1-42}$. (E) and (J) were a single cell image respectively according to (D) and (I) fields taken under 400 × magnification. The white arrows pointed out the view of 400 × images where are selected from 100 × ones.

3. Results

3.1. Permeability, cytotoxicity and pro-inflammation of AgNPs in neural cells

The zeta potential of the 3–5 nm AgNPs used in this study was −4.2 mV in culture medium. The 3–5 nm AgNPs (12.5 μg/ml) can cross the cell membrane of N2a cells detectable under a polarizing microscope (Fig. 1). The cell proliferation of ALT, BV-2 and N2a cells exposed to AgNPs (0.5, 1, 5, 10 and 12.5 μg/ml) and LPS (0.2, 2 μg/ml) for 24 h were shown in Fig. 2. The cell proliferation was decreased in ALT cells (0.5, 1, 10 and 12.5 μg/ml) and N2a cells (12.5 μg/ml) but not differently changed in BV-2 cells after AgNPs exposure. LPS decreased cell proliferation obviously in ALT cells (2 μg/ml) and BV-2 cells (0.2 μg/ml). Additionally, the IL-1β secretion of ALT, BV-2 and N2a cells was detected after 24 h AgNPs exposure (Fig. 3). IL-1β protein was significantly increased in BV-2 cells after 12.5 μg/ml AgNPs exposure.

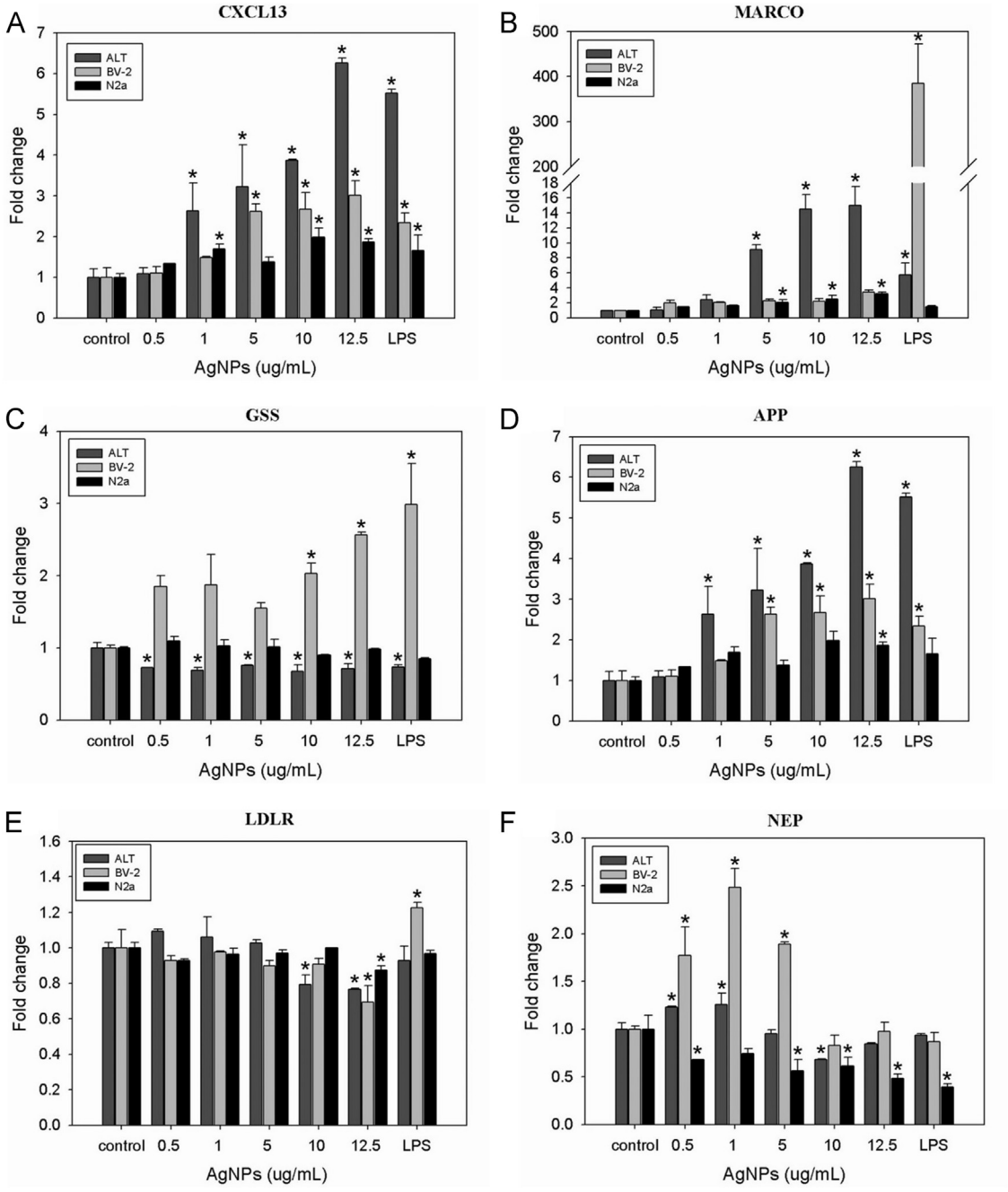

Fig. 6. Quantitative changes of (A) *CXCL13*, (B) *MARCO*, (C) *GSS*, (D) *APP*, (E) *LDLR* and (F) *NEP* gene expression in the neural cells with the treatment of 3–5 nm AgNPs or LPS. Neural cells were treated with different concentration of 3–5 nm AgNPs (0.5, 1, 5, 10 and 12.5 μg/ml) and LPS (ALT 2 μg/ml, BV-2 0.2 μg/ml and N2a 2 μg/ml) for 24 h. The data were presented as mean ± SD ($n=3$). Asterisk indicates significant difference at $p<0.05$ compared with control. ALT: astrocyte, BV-2: microglia, and N2a: neuron cells.

3.2. *Aβ amyloid deposition in neural cells after AgNPs exposure*

The immunofluorescence images revealed that $A\beta_{1-40}$ (Fig. 4) and $A\beta_{1-42}$ (Fig. 5) proteins were inducible to generate after AgNPs exposure 12.5 μg/ml in N2a cells, and detectable in a fluorescence microscope.

3.3. *Gene expression of neural cells in exposure to AgNPs*

LPS induced the expression of *CXCL13* and *MARCO* genes for inflammatory process and phagocytosis. The gene expression of *CXCL13* and *MARCO* were increased in ALT, BV-2 and N2a cells at the higher dose of AgNPs (5, 10 and 12.5 μg/ml) (Fig. 6A and B). The *GSS* mRNA level was significantly decreased in ALT cells (0.5, 1, 5, 10 and 12.5 μg/ml) and increased in BV-2 cells (10 and 12.5 μg/ml) after AgNPs exposure (Fig. 6C). On the other hand, the gene expression of AD process related genes such as *APP*, *LDLR* and *NEP* were also altered in exposure to AgNPs. The gene expression of *APP* was elevated in ALT, BV-2 (5, 10 and 12.5 μg/ml) and N2a (12.5 μg/ml) cells (Fig. 6D). On the contrary, the decreased *LDLR* mRNA level was observed in 12.5 μg/ml AgNPs-treated ALT, BV-2 and N2a cells (Fig. 6E). *NEP* gene expression also reduced significantly in N2a cells exposed to AgNPs (Fig. 6F).

3.4. *Protein determination of neural cells in exposure to AgNPs*

The protein levels of APP, LDLR and NEP were determined after N2a cells exposed to 1, 5, 10, 12.5 and 15 μg/ml AgNPs,

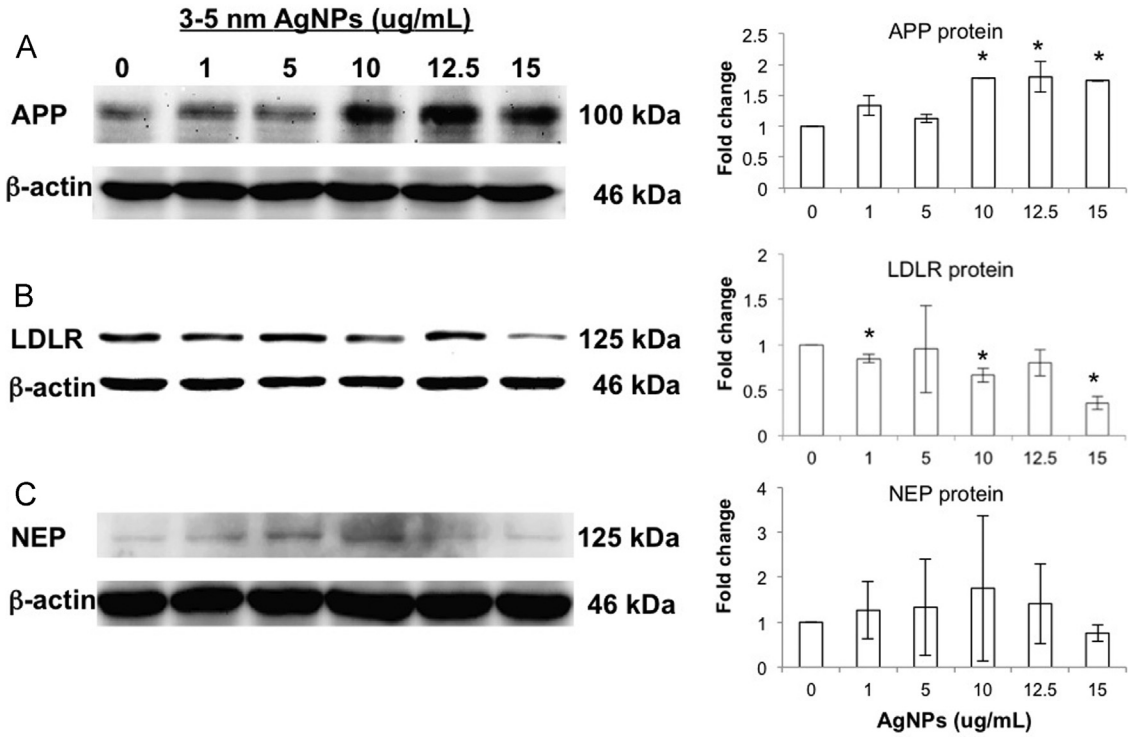

Fig. 7. Protein levels of APP, LDLR and NEP in N2a cells after AgNPs exposure. The total protein were 40, 40 and 100 μg individually loaded for immnunoblotting to determine (A) APP, (B) LDLR and (C) NEP in N2a cells exposed to 1, 5, 10, 12.5 and 15 μg/ml AgNPs for 24 h, and quantified by ImageJ. Asterisk indicates significant difference at $p < 0.05$ compared with control.

respectively. APP levels were obviously induced in exposure to 10, 12.5 and 15 μg/ml AgNPs (Fig. 7A). LDLR levels were significantly reduced after exposure to 1, 10 and 15 μg/ml AgNPs (Fig. 7B). The level of NEP protein was increased after AgNPs and returned to the steady state as control group (Fig. 7C).

4. Discussion

This study found that 3–5 nm AgNPs can cross the cell membrane (Fig. 1), induced IL-1β secretion for inflammatory response (Fig. 3), and accelerate $A\beta_{1-40}$ (Fig. 4) and $A\beta_{1-42}$ (Fig. 5) generation and deposition. AgNPs exposure (5, 10, 12.5 μg/ml) induced the gene expression of *CXCL13*, *MARCO* and *GSS* for inflammatory response and oxidative stress (Fig. 6). Besides, AgNPs exposure increased the gene expression and protein level of APP for Aβ generation, and reduced LDLR and NEP for Aβ uptake/transporter and Aβ degradation (Figs. 6 and 7). These findings suggested that AgNPs exposure potentially caused neurodegenerative disorder progression underlying Aβ deposition.

4.1. AgNPs exposure induced inflammatory response in mouse neural cells

This study found that AgNPs crossed the cell membrane of neuron cells and mostly distributed in the cytoplasm (Fig. 1), and induced IL-1β secretion (Fig. 3) for inflammatory response in neural cells (astrocytes, microglia and neuron cells). AgNPs and iron oxide nanoparticles in astrocytes are internalized by endocytotic uptake processes into cellular vesicles to respectively release Ag and ferrous iron and induce ROS generation and inflammation (Hohnholt et al., 2013). Prasad et al. (2013) indicated that AgNPs have a higher rate of cellular uptake compared with $AgNO_3$ and cause oxidative stress and inflammatory response in liver HepG2 cells. Moreover, AgNPs can enter the brain through the olfactory nerve, and the toxic effect of AgNPs is stronger than silver ions because ions are consumed before reaching the cell membrane (Wijnhoven et al., 2009, Quadros and Marr, 2010). Besides, in the analysis of Mouse Oxidative Stress and Antioxidant Defense Arrays, male C57BL/6N mice administered with 25 nm AgNPs change the expression of oxidative stress associated genes in the caudate, frontal cortex and hippocampus (Rahman et al., 2009).

The results of this study indicated that AgNPs activated stress-responsive gene *GSS* and immune reaction genes *CXCL13* and *MARCO*. AgNPs induces inflammatory cytokine TNF-α release, ROS and endoplasmatic reticulum (ER) stress response in zebrafish liver cells (Christen et al., 2013). Cha et al. (2008) found the AgNPs-treated liver cells have the up-regulated gene expression of *CXCL13* and *MARCO* to induce apoptosis and inflammation. Moreover, chemokine C–C motif ligand (CCL) 2 can activate resident microglias in the brain to recruit peripheral macrophages and increase chemokine family *CCL24* gene expression (Selenica et al., 2013). Kang et al. (2012) reported that 7.5 ± 2.5 nm AgNPs evoke ROS generation and increase a major cellular thiol antioxidant GSH level in human renal proximal tubular epithelial HK-2 cells. Importantly, the diameter of 20 and 40 nm AgNPs (10 and 20 μg/ml) can lead to mixed primary cortical neural cells increase the level of ROS in accompanied with calcium rises, and the smaller AgNPs have stronger cytotoxicity than bigger ones (Haase et al., 2012).

4.2. AgNPs exposure changed gene expression and protein level of amyloid plaque deposition in mouse neuron cells

Neuroinflammation and beta-amyloid deposition led to memory impairment in Alzheimer's disease transgenic mice (Xu et al., 2014). According to above studies, we inferred that chronic ROS increase and unbalance calcium level in neural cells may cause AD neurodegenerative disorder. This study observed that AgNPs caused Aβ amyloid plaque deposition in mouse neuron N2a cells

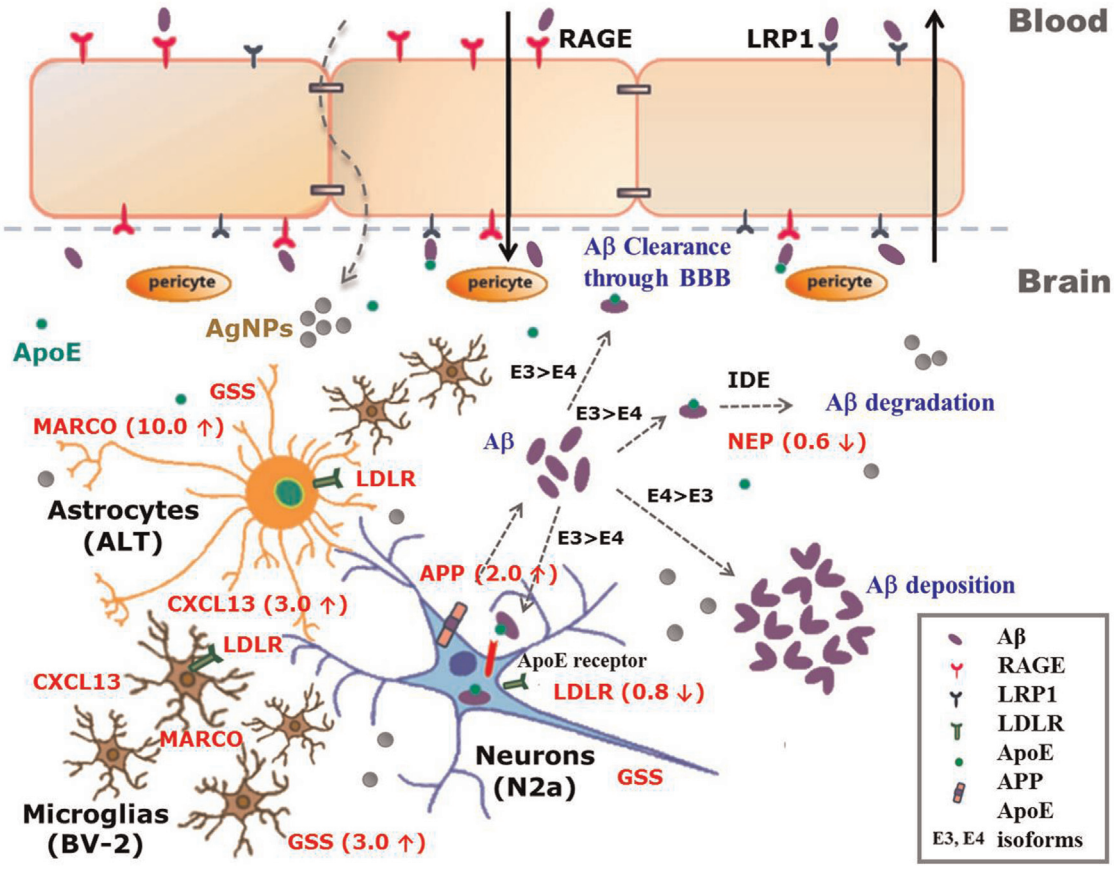

Fig. 8. A schematic diagram of AgNPs exposure in brain neural cells to alter gene expression potentially resulting in the progression of Aβ plaque deposition and pathological feature of Alzheimer's disease. AgNPs can enter across neuronal cell membrane and induce the gene expression of *CXCL13*, *MARCO* and *GSS* in response to inflammatory reaction and oxidative stress. Sequentially, *APP* gene is activated for Aβ amyloid production, ApoE transport is influenced to accelerate Aβ aggregation, and *NEP* and *LDLR* genes are reduced for Aβ deposition. In addition, the Aβ proteins are increased through the up-regulated.*RAGE* and down-regulated.*LRP1* expression, and the dramatically enhanced level of Aβ proteins lead to decrease *IDE* and *NEP* gene expression to accelerate Aβ deposition. The AgNPs-induced. neuroinflammatory response and Aβ amyloid deposition might evolve neurodegenerative Alzheimer's disease. The number and arrow marked in red are fold-change. levels and up-/down-regulation. of gene expression.

(Figs. 4 and 5). Furthermore, this study determined the gene expression corresponding to Aβ generation and deposition in neural cells treated with AgNPs (Fig. 6).

The ability of insoluble 40–42 peptides of Aβ amyloid has been considered more rapidly aggregation and more neurotoxicity in AD progression (Landau et al., 2013). In this study, AgNPs exposure can induce $Aβ_{1-40}$ and $Aβ_{1-42}$ peptides aggregation in neural cells (Figs. 4 and 5). Additionally, the gene expression (Fig. 6) and protein level (Fig. 7) of Aβ amyloid generation and deposition relevant to AD progression have been explored after AgNPs exposure. AgNPs induced the expression of *APP*, and otherwise, attenuated *NEP* and *LDLR* for the potential effect on Aβ deposition. APP protein is an integral membrane glycoprotein expressing in the brain and central nervous system, and Aβ amyloid is produced by sequential cleavage of APP by β-secretase and γ-secretase (Dong et al., 2012). The increased APP and β-secretase levels lead to increase Aβ amyloid formation and aggregation potentially for neurodegenerative disease (Meraz–Rios et al., 2013). The results of this study suggested that AgNPs led to up-regulate the gene expression of *APP*, and down-regulate Aβ uptake gene *LDLR* and Aβ degradation gene *NEP*. LDLR can enhance Aβ uptake and degradation to regulate Aβ levels in the mouse brain (Basak et al., 2012). Cao et al. (2006) indicated that Aβ deposition accompanies with the increased ApoE expression in *LDLR*-deficient Tg2576 mice. *LDLR*-deficient Tg2576 mice have disorders in hypercholesterolemia, age-dependent cerebral β-amyloidosis and spatial learning deficits after Aβ deposition. Thus, LDLR plays an important role in amyloidosis and the development of Alzheimer-type learning impairment. NEP is the major protease involved in Aβ degradation. The decreased *NEP* mRNA level is observed in AD patients (Wang et al., 2010). AD patients have the significantly lower *NEP* mRNA and protein levels in the brain with high Aβ plaque burdens (Park et al., 2013).

4.3. The potential mechanism of AD pathogenesis in mouse neural cells exposure to AgNPs

This study observed that AgNPs activated the gene expression of *GSS*, *CXCL13* and *MARCO* for stress-response and immune reaction, and induced *APP* and attenuated *NEP* and *LDLR* genes for the potential effect on Aβ deposition. Regarding to our findings in this study, a schematic diagram illustrated in Fig. 8 described that AgNPs exposure in brain neural cells results in gene expression changes underlying the possible progression of Aβ plaque deposition for AD pathological feature. Inflammation elicits Aβ deposition via the activated microglia cells (Cameron and Landreth, 2010). This present study found AgNPs can enter into N2a cells and induce inflammatory response and Aβ deposition. The gene expression of *CXCL13*, *MARCO* and *GSS* in ALT, BV-2 and N2a cells are enhanced to defense against AgNPs-induced inflammatory reaction and oxidative stress. The APP protein is assembled from amino acids using information encoded in *APP* gene, which can be cleaved by α-secretase, β-secrease and γ-secrease to produce different length of Aβ peptides such as $Aβ_{1-40}$ or $Aβ_{1-42}$. Both of

receptor for advanced glycation end product (RAGE) and low density lipoprotein receptor-related protein 1 (LRP1) are Aβ receptors able to bind Aβ or ApoE/Aβ complexes. RAGE transports Aβ proteins from blood to brain; in contrast, LRP1 transfers Aβ proteins from brain to blood (Kanekiyo et al., 2012; Han et al., 2011). LDLR plays the main regulator with ApoE in CNS trafficking and breaking the balance of Aβ levels. The different isoforms of ApoE play different function, the neutral ApoE3 and protective ApoE2 can support Aβ transport or degradation, and the AD-risk factor ApoE4 accelerates Aβ aggregation for amyloid plaque formation (Morris et al., 2010). There are sequential pathways to balance the Aβ levels in the brain, e.g., Aβ clearance through BBB via RAGE and LRP1, Aβ degradation via NEP protease and insulin-degrading enzyme (IDE), and Aβ deposition internalized in neural cells via ApoE receptor when ApoE3 > ApoE4. AgNPs can activate *APP* gene to generate Aβ amyloid, and disturb ApoE transport and reduce *NEP* and *LDLR* expression to accelerate Aβ aggregation and deposition in neural cells.

5. Conclusion

In summary, this study identified 3–5 nm AgNPs can enter in mouse neural cells to induce pro-inflammatory cytokine secretion and increase Aβ amyloid deposition in response to the changes of gene expression in inflammatory response, oxidative stress and Aβ degradation. These results suggested that AgNPs-induced neuroinflammatory response and Aβ deposition might evolve the progress of neurodegenerative disorders. It is necessary to note the daily usage of silver nanoparticles.

Acknowledgment

We thank Gold Nanotech, Inc., Taiwan for providing AgNP materials in this collaborative research.

References

Basak, J.M., Verghese, P.B., Yoon, H., Kim, J., Holtzman, D.M., 2012. Low-density lipoprotein receptor represents an apolipoprotein E-independent pathway of Abeta uptake and degradation by astrocytes. J. Biol. Chem. 287, 13959–13971.
Cameron, B., Landreth, G.E., 2010. Inflammation, microglia, and Alzheimer's disease. Neurobiol. Dis. 37, 503–509.
Cao, D., Fukuchi, K., Wan, H., Kim, H., Li, L., 2006. Lack of LDL receptor aggravates learning deficits and amyloid deposits in Alzheimer transgenic mice. Neurobiol. Aging 27, 1632–1643.
Cha, K., Hong, H.W., Choi, Y.G., Lee, M.J., Park, J.H., Chae, H.K., Ryu, G., Myung, H., 2008. Comparison of acute responses of mice livers to short-term exposure to nano-sized or micro-sized silver particles. Biotechnol. Lett. 30, 1893–1899.
Christen, V., Capelle, M., Fent, K., 2013. Silver nanoparticles induce endoplasmatic reticulum stress response in zebrafish. Toxicol. Appl. Pharmacol. 272, 519–528.
Dong, S., Duan, Y., Hu, Y., Zhao, Z., 2012. Advances in the pathogenesis of Alzheimer's disease: a re-evaluation of amyloid cascade hypothesis. Transl. Neurodegener. 1, 18.
Dziendzikowska, K., Gromadzka-Ostrowska, J., Lankoff, A., Oczkowski, M., Krawczynska, A., Chwastowska, J., Sadowska-Bratek, M., Chajduk, E., Wojewodzka, M., Dusinska, M., Kruszewski, M., 2012. Time-dependent biodistribution and excretion of silver nanoparticles in male Wistar rats. J. Appl. Toxicol. 32, 920–928.
El-Amouri, S.S., Zhu, H., Yu, J., Gage, F.H., Verma, I.M., Kindy, M.S., 2007. Neprilysin protects neurons against Abeta peptide toxicity. Brain Res. 1152, 191–200.
Eom, H.J., Choi, J., 2010. p38 MAPK activation, DNA damage, cell cycle arrest and apoptosis as mechanisms of toxicity of silver nanoparticles in Jurkat T cells. Environ. Sci. Technol. 44, 8337–8342.
Foldbjerg, R., Dang, D.A., Autrup, H., 2011. Cytotoxicity and genotoxicity of silver nanoparticles in the human lung cancer cell line, A549. Arch. Toxicol. 85, 743–750.
Gaiser, B.K., Hirn, S., Kermanizadeh, A., Kanase, N., Fytianos, K., Wenk, A., Haberl, N., Brunelli, A., Kreyling, W.G., Stone, V., 2013. Effects of silver nanoparticles on the liver and hepatocytes in vitro. Toxicol. Sci. 131, 537–547.
Haase, A., Rott, S., Mantion, A., Graf, P., Plendl, J., Thunemann, A.F., Meier, W.P., Taubert, A., Luch, A., Reiser, G., 2012. Effects of silver nanoparticles on primary mixed neural cell cultures: uptake, oxidative stress and acute calcium responses. Toxicol. Sci. 126, 457–468.
Han, S.H., Kim, Y.H., Mook-Jung, I., 2011. RAGE: the beneficial and deleterious effects by diverse mechanisms of actions. Mol. Cells 31, 91–97.
Hohnholt, M.C., Geppert, M., Luther, E.M., Petters, C., Bulcke, F., Dringen, R., 2013. Handling of iron oxide and silver nanoparticles by astrocytes. Neurochem. Res. 38, 227–239.
Kanekiyo, T., Liu, C.C., Shinohara, M., Li, J., Bu, G., 2012. LRP1 in brain vascular smooth muscle cells mediates local clearance of Alzheimer's amyloid-beta. J. Neurosci. 32, 16458–16465.
Kang, S.J., Lee, Y.J., Lee, E.K., Kwak, M.K., 2012. Silver nanoparticles-mediated G_2/M cycle arrest of renal epithelial cells is associated with NRF2-GSH signaling. Toxicol. Lett. 211, 334–341.
Koike, S., Ogasawara, Y., Shibuya, N., Kimura, H., Ishii, K., 2013. Polysulfide exerts a protective effect against cytotoxicity caused by t-buthylhydroperoxide through Nrf2 signaling in neuroblastoma cells. FEBS Lett. 587, 3548–3555.
Komine, H., Kuhn, L., Matsushita, N., Mule, J.J., Pilon-Thomas, S., 2013. Examination of MARCO activity on dendritic cell phenotype and function using a gene knockout mouse. PLoS One 8, e67795.
Kulthong, K., Srisung, S., Boonpavanitchakul, K., Kangwansupamonkon, W., Manirratanachote, R., 2010. Determination of silver nanoparticle release from antibacterial fabrics into artificial sweat. Part Fibre Toxicol. 7, 8.
Landau, S.M., Lu, M., Joshi, A.D., Pontecorvo, M., Mintun, M.A., Trojanowski, J.Q., Shaw, L.M., Jagust, W.J., Alzheimer's Disease Neuroimaging, I., 2013. Comparing positron emission tomography imaging and cerebrospinal fluid measurements of beta-amyloid. Ann. Neurol. 74, 826–836.
Lee, D.Y., Fortin, C., Campbell, P.G., 2005. Contrasting effects of chloride on the toxicity of silver to two green algae, Pseudokirchneriella subcapitata and *Chlamydomonas reinhardtii*. Aquat. Toxicol. 75, 127–135.
Loo, S.L., Fane, A.G., Lim, T.T., Krantz, W.B., Liang, Y.N., Liu, X., Hu, X., 2013. Superabsorbent cryogels decorated with silver nanoparticles as a novel water technology for point-of-use disinfection. Environ. Sci. Technol. 47, 9363–9371.
Meraz-Rios, M.A., Toral-Rios, D., Franco-Bocanegra, D., Villeda-Hernandez, J., Campos-Pena, V., 2013. Inflammatory process in Alzheimer's Disease. Front. Integr. Neurosci. 7, 59.
Morris, J.C., Roe, C.M., Xiong, C., Fagan, A.M., Goate, A.M., Holtzman, D.M., Mintun, M.A., 2010. APOE predicts amyloid-beta but not tau Alzheimer pathology in cognitively normal aging. Ann. Neurol. 67, 122–131.
Nakajima, T., Amanuma, R., Ueki-Maruyama, K., Oda, T., Honda, T., Ito, H., Yamazaki, K., 2008. CXCL13 expression and follicular dendritic cells in relation to B-cell infiltration in periodontal disease tissues. J. Periodontal. Res. 43, 635–641.
Park, M.H., Lee, J.K., Choi, S., Ahn, J., Jin, H.K., Park, J.S., Bae, J.S., 2013. Recombinant soluble neprilysin reduces amyloid-beta accumulation and improves memory impairment in Alzheimer's disease mice. Brain Res. 1529, 113–124.
Prasad, R.Y., Mcgee, J.K., Killius, M.G., Suarez, D.A., Blackman, C.F., Demarini, D.M., Simmons, S.O., 2013. Investigating oxidative stress and inflammatory responses elicited by silver nanoparticles using high-throughput reporter genes in HepG2 cells: effect of size, surface coating, and intracellular uptake. Toxicol. In Vitro 27, 2013–2021.
Quadros, M.E., Marr, L.C., 2010. Environmental and human health risks of aerosolized silver nanoparticles. J. Air Waste Manag. Assoc. 60, 770–781.
Rahman, M.F., Wang, J., Patterson, T.A., Saini, U.T., Robinson, B.L., Newport, G.D., Murdock, R.C., Schlager, J.J., Hussain, S.M., Ali, S.F., 2009. Expression of genes related to oxidative stress in the mouse brain after exposure to silver-25 nanoparticles. Toxicol. Lett. 187, 15–21.
Ribeiro, F., Gallego-Urrea, J.A., Jurkschat, K., Crossley, A., Hassellov, M., Taylor, C., Soares, A.M., Loureiro, S., 2013. Silver nanoparticles and silver nitrate induce high toxicity to *Pseudokirchneriella subcapitata*, *Daphnia magna* and *Danio rerio*. Sci. Total Environ. 466–467, 232–241.
Selenica, M.L., Alvarez, J.A., Nash, K.R., Lee, D.C., Cao, C., Lin, X., Reid, P., Mouton, P.R., Morgan, D., Gordon, M.N., 2013. Diverse activation of microglia by chemokine (C–C motif) ligand 2 overexpression in brain. J. Neuroinflammation 10, 86.
Sharma, H.S., Sharma, A., 2012. Neurotoxicity of engineered nanoparticles from metals. CNS Neurol. Disord. Drug Targets 11, 65–80.
Singh, R.P., Ramarao, P., 2012. Cellular uptake, intracellular trafficking and cytotoxicity of silver nanoparticles. Toxicol. Lett. 213, 249–259.
Smith, M.P., Cass, W.A., 2007. Oxidative stress and dopamine depletion in an intrastriatal 6-hydroxydopamine model of Parkinson's disease. Neuroscience 144, 1057–1066.
Sofroniew, M.V., Vinters, H.V., 2010. Astrocytes: biology and pathology. Acta Neuropathol. 119, 7–35.
Tang, J., Xiong, L., Wang, S., Wang, J., Liu, L., Li, J., Yuan, F., Xi, T., 2009. Distribution, translocation and accumulation of silver nanoparticles in rats. J. Nanosci. Nanotechnol. 9, 4924–4932.
Tang, J., Xiong, L., Zhou, G., Wang, S., Wang, J., Liu, L., Li, J., Yuan, F., Lu, S., Wan, Z., Chou, L., Xi, T., 2010. Silver nanoparticles crossing through and distribution in the blood–brain barrier in vitro. J. Nanosci. Nanotechnol. 10, 6313–6317.
Tappin, A.D., Barriada, J.L., Braungardt, C.B., Evans, E.H., Patey, M.D., Achterberg, E.P., 2010. Dissolved silver in European estuarine and coastal waters. Water Res. 44, 4204–4216.
Verano-Braga, T., Miethling-Graff, R., Wojdyla, K., Rogowska-Wrzesinska, A., Brewer, J.R., Erdmann, H., Kjeldsen, F., 2014. Insights into the cellular response triggered by silver nanoparticles using quantitative proteomics. ACS Nano 8, 2161–2175.
Wang, S., Wang, R., Chen, L., Bennett, D.A., Dickson, D.W., Wang, D.S., 2010. Expression and functional profiling of neprilysin, insulin-degrading enzyme, and

endothelin-converting enzyme in prospectively studied elderly and Alzheimer's brain. J. Neurochem. 115, 47–57.
Wang, Y., Wang, B., Zhu, M.T., Li, M., Wang, H.J., Wang, M., Ouyang, H., Chai, Z.F., Feng, W.Y., Zhao, Y.L., 2011. Microglial activation, recruitment and phagocytosis as linked phenomena in ferric oxide nanoparticle exposure. Toxicol. Lett. 205, 26–37.
Wei, J., Gabrusiewicz, K., Heimberger, A., 2013. The controversial role of microglia in malignant gliomas. Clin. Dev. Immunol. 2013, 285246.
Weiss, N., Miller, F., Cazaubon, S., Couraud, P.O., 2009. The blood–brain barrier in brain homeostasis and neurological diseases. Biochim. Biophys. Acta 1788, 842–857.
Wijnhoven, S.W.P., Peijnenburg, W.J.G.M., Herberts, C.A., Hagens, W.I., Oomen, A.G., Heugens, E.H.W., Roszek, B., Bisschops, J., Gosens, I., Van De Meent, D., Dekkers, S., De Jong, W.H., Van Zijverden, M., Sips, A.J.A.M., Geertsma, R.E., 2009. Nano-silver a review of available data and knowledge gaps in human and environmental risk assessment. Nanotoxicology 3, 109–138.
Xu, F., Piett, C., Farkas, S., Qazzaz, M., Syed, N.I., 2013. Silver nanoparticles (AgNPs) cause degeneration of cytoskeleton and disrupt synaptic machinery of cultured cortical neurons. Mol. Brain 6, 29.
Xu, P.X., Wang, S.W., Yu, X.L., Su, Y.J., Wang, T., Zhou, W.W., Zhang, H., Wang, Y.J., Liu, R.T., 2014. Rutin improves spatial memory in Alzheimer's disease transgenic mice by reducing Aβ oligomer level andattenuating oxidative stress and neuroinflammation. Behav. Brain Res. 264, 173–180.